Journal of Solid State Chemistry **166,** 171–176 (2002)
doi:10.1006/jssc.2002.9577, available online at http://www.idealibrary.com on IDEAL®

Structural and Transport Properties of $Mg_{1-x}Mn_xMn_2O_{4\pm\delta}$ Spinels

Lorenzo Malavasi,[1] Paolo Ghigna, Gaetano Chiodelli, Giorgio Maggi, and Giorgio Flor

INSTM, C.S.T.E./CNR, Dipartimento di Chimica Fisica "M. Rolla", Università di Pavia, I-27100 Pavia, Italy

Received December 12, 2001; in revised form February 19, 2002; accepted March 1, 2002

The synthesis and structural properties of $Mg_{1-x}Mn_{2+x}O_4$, for $0 \leq x \leq 1$ are described. Complete miscibility in the solid state exists for this system. For the material with the correct stoichiometry, i.e. $MgMn_2O_4$, the effect of temperature on the cation distribution was investigated: above 600°C the inversion degree (*m*) starts increasing. The electrical conductivity shows a small dependence on $P(O_2)$ which is consistent with the small oxygen non-stoichiometry determined by means of thermogravimetry. The main contribution to the transport properties arises from the inversion equilibrium. Two distinct conductivity regimes, below and above the inversion threshold, can be assumed to explain the electrical conductivity and thermoelectric power results.

Key Words: **$MgMn_2O_4$ spinel; X-ray diffraction; inversion; electrical conductivity.**

1. INTRODUCTION

In recent years, manganese-containing oxides have received renewed interest after the discovery, in lanthanum manganites, of extremely high magnetoresistance values. Many other phases, such as layered manganites, have been also studied since the presence of manganese ions with different oxidation states introduce novel and interesting properties. We started a systematic characterization of structural, transport and magnetic properties of manganese spinel oxides of the general formula AMn_2O_4 (A = Cd, Mg, Zn, Mn) that are materials of interest both for fundamental and industrial research. In particular, some compounds of this class turned out to be promising materials for mixed potential oxygenic gas (such as NO_x) sensors (1–3). From a structural point of view, AMn_2O_4 (A = Cd, Mg, Zn, Mn) spinels, in contrast to the cubic $LiMn_2O_4$ spinel, show a tetragonally distorted structure (hausmannite-like structure) due to the cooperative Jahn–Teller distortion associated with the Mn(III) ions that fill the octahedral sites of the oxygen ion closed packed arrangement.

[1]To whom correspondence should be addressed. E-mail: malavasi@chifis.unipv.it.

In a previous investigation (4, 5) we studied in detail the transport properties of $Cd_{1-x}Mn_xMn_2O_4$ spinel. By means of X-ray absorption spectroscopy (XAS) we could show that cadmium deficiency is compensated by Mn(II) ions in the tetrahedral sites of the spinel structure. For applicative purposes (i.e. as sensor material), anyway, less toxic compounds should be considered. For this reason we started a deep characterization of the $Mg_{1-x}Mn_{2+x}O_4$ system, for $0 \leq x \leq 1$, which has been scarcely studied in the previous literature. There are indeed, some papers dealing with the study of cation distribution in $MgMn_2O_4$. For this spinel, in contrast to $ZnMn_2O_4$ and $CdMn_2O_4$, there is a greater tendency for the inversion process to occur. In the present case, part of the magnesium ions can be found in the octahedral sites already at room temperature. The inversion degree is usually expressed by a parameter, m, and following the spinel formula is written as $(A_{1-m}B_m)^{tet}[A_mB_{2-m}]^{oct}O_4$. However, there are some conflicting reports about the inversion degree for this spinel. In fact, while neutron diffraction data point to an inversion degree at room temperature close to 0.2 (6), X-ray diffraction experiments could reveal only a much smaller figure, close to 0.02 (7). It is therefore clear that further experimental investigations are highly desirable.

In this paper we present an experimental study of the synthesis, structure, defect equilibria and transport properties of $MgMn_2O_4$. In addition, the structural properties of the $Mg_{1-x}Mn_{2+x}O_4$ solid solutions (with $0 \leq x \leq 1$) were also considered in order to define the homogeneity range of the solid solutions and to study the effect of magnesium replacement in Mn_3O_4, which has the same tetragonal distorted spinel structure.

2. EXPERIMENTAL

$Mg_{1-x}Mn_xMn_2O_4$ samples were synthesized by solid-state reaction of stoichiometric amounts of Mn_2O_3 (Aldrich, 99.999%) and MgO (Aldrich, 99.9%). Pellets were prepared from the thoroughly mixed powders and allowed to react at 1200°C for a total time of at least 6 days during which they were re-ground and re-pelletized at least twice.

0022-4596/02 $35.00

X-ray powder diffraction (XRPD) and electron microprobe analysis (EMPA) inspections were performed to check the phase purity of the obtained materials. Samples employed in the electrical conductivity measurements have been slowly cooled down to room temperature (10°C/min).

X-ray powder diffraction patterns were acquired on a Philips 1710 diffractometer equipped with a Cu anticathode, adjustable divergence slit, graphite monochromator on the diffracted beam and proportional detector. The lattice constants were determined by minimizing the weighted squared difference between calculated and experimental Q_i values, where $Q_i = 4\sin^2\theta_i/\lambda_i^2$ and weight $= \sin(2\theta_i)^{-2}$. Instrumental aberrations were considered by inserting additional terms into the linear least-squares fitting model (8). EMPA measurements were carried out using an ARL SEMQ scanning electron microscope, performing at least 10 measurements in different regions of each sample. According to EMPA and XRPD, the above synthetic procedure gave single-phase materials; in addition, for each composition the prepared materials were found to be homogeneous in the chemical composition, which was met in fair agreement with the nominal one.

Thermogravimetric measurements were performed under different atmospheres (obtained by flowing into the apparatus certified mixtures of oxygen in nitrogen) with a TA 2905 thermal analysis system. Electrochemical experiments were executed in a home-made apparatus that permits measurements to be taken up to 1000°C and under selected atmospheres. Impedance spectroscopy (IS) measurements were carried out by means of a Solartron 1170 frequency response analyzer, equipped with an active guard for minimizing noise and capacitive effects of cables (9). For the measurements, samples were prepared in the form of disk-shaped pellets and platinum electrodes were sputtered on the flat surfaces. DC conductivity measurements were performed by means of a Solartron 1286 galvanostat/voltmeter, using the four-probe DC method, on samples shaped in the form of parallelepipeds. The samples employed in the electrical conductivity measurements have been sintered in order to achieve a densification greater than 90%. Thermoelectric power measurements were carried out by means of the electrochemical cell described in a previous work (10) on disk-shaped samples.

A direct Rietveld refinement on the acquired XRPD pattern for obtaining the inversion degree did not give sensible results. This is at least partly due to the huge amount of correlation between the inversion degree and the Debye–Waller factors. Thus, for obtaining the m parameter as a function of temperature, we used the following procedure. We started a FullProf (11) refinement of the XRPD patterns acquired at different temperatures with an arbitrary inversion degree which was kept fixed and in addition was arbitrarily assumed to be equal for all the temperatures. This has been done since whatever was the actual value of the inversion degree, its variation with temperature is quite small. In this step, we use as refinement parameter one isotropic thermal factor (B) arbitrarily assumed to be equal for all the atoms. We repeated this procedure for different inversion degrees. This step, therefore, gives a mean inversion degree (with respect to temperature) and for each temperature a mean Debye–Waller factor. Then using this thermal factor, we simulated the XRPD patterns for different inversion degrees. Simulation of XRPD patterns was accomplished by means of PowderCell 2.2 (12). Then we used the ratio between the intensities of (211) reflection, the reflection which is relatively independent of the inversion degree, and the (101) reflection which, on the contrary, has a large dependence on the inversion degree. A comparison between these calculated ratios and the experimental ones gives the inversion degree, m, as a function of temperature. We can estimate the error in m obtained by this procedure to be around 5%.

3. RESULTS

Figure 1 reports the indexed X-ray powder pattern for $MgMn_2O_4$. All the synthesized samples of the $Mg_{1-x}Mn_{2+x}O_4$ system, for $0 \le x \le 1$, can be indexed as the tetragonal distorted spinel structure of Mn_3O_4 (13); this clearly indicates the existence of a complete miscibility in the solid state between Mn_3O_4 and $MgMn_2O_4$. Figures 2 and 3 present the lattice constant, cell volume and tetragonal distortion for the samples prepared. The lattice constant values are reported in Table 1. The tetragonal distortion is expressed as c/a' where $a' = a\sqrt{2}$, thus referring to the face-centered pseudocubic unit cell constructed along the diagonal of the tetragonal one. As can be clearly seen, by increasing the magnesium content the lattice parameters,

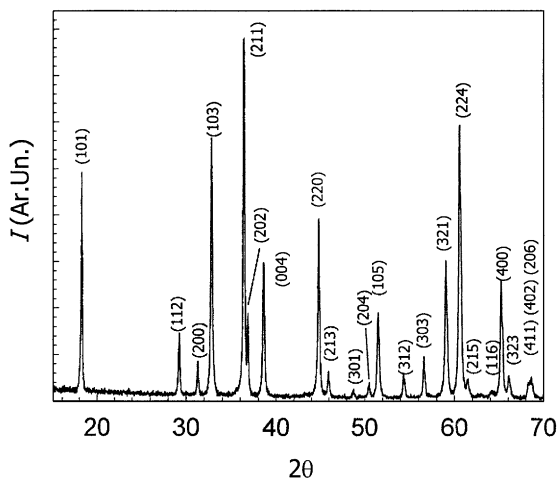

FIG. 1. Indexed XRDP pattern of $MgMn_2O_4$.

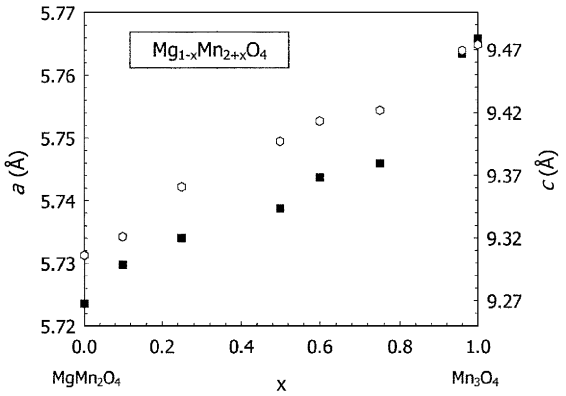

FIG. 2. Lattice constants in $Mg_{1-x}Mn_{2+x}O_4$ for $0 \le x \le 1$. White diamonds: c; black squares: a, b.

TABLE 1
Lattice Constant Values for the Samples Considered

Samples	a(Å)	a'(Å)	c(Å)
Mn_3O_4	5.767(1)	8.155(1)	9.474(2)
$Mg_{0.04}Mn_{2.96}O_4$	5.763(2)	8.149(3)	9.470(3)
$Mg_{0.25}Mn_{2.75}O_4$	5.753(1)	8.134(1)	9.432(1)
$Mg_{0.4}Mn_{2.6}O_4$	5.744(1)	8.122(1)	9.413(2)
$Mg_{0.5}Mn_{2.5}O_4$	5.739(1)	8.115(1)	9.397(1)
$Mg_{0.75}Mn_{2.25}O_4$	5.734(1)	8.109(1)	9.361(1)
$Mg_{0.9}Mn_{2.1}O_4$	5.730(1)	8.108(1)	9.321(2)
$MgMn_2O_4$	5.724(1)	8.094(1)	9.306(2)
$MgMn_2O_4$, 400°C	5.734(1)	8.109(1)	9.359(1)
$MgMn_2O_4$, 600°C	5.736(1)	8.111(1)	9.373(1)
$MgMn_2O_4$, 800°C	5.746(1)	8.125(1)	9.381(1)

unit-cell volume and the tetragonal distortion reduce. The almost linear trend of the lattice parameters confirms the existence of a complete range of solid solutions between $x = 0$ and 1. This result is in agreement with electron paramagnetic resonance (EPR) measurements that we performed on this system (14). An analogous investigation carried out on $Cd_{1-x}Mn_{2+x}O_4$ showed that all the EPR signals at room temperature in $CdMn_2O_4$ can be attributed to Mn(III) in a distorted octahedral environment (15). It should be noted that Mn(III) (d^4) is a non-Kramers ion, and an EPR signal can be obtained due to the Jahn–Teller distortion of the coordination octahedron. The Mn(III) EPR signal in $CdMn_2O_4$ is completely analogous to that in $MgMn_2O_4$, with the exception of a slight decrease in intensity in $MgMn_2O_4$. This decrease in intensity can be attributed to the migration of some Mn(III) from the octahedral to the tetrahedral sites that is to the presence of a partial inversion also for those samples slowly cooled to RT. Concerning the inversion degree of $MgMn_2O_4$ spinel, literature data of neutron diffraction experiments suggest an inversion degree, m, around 0.2 (6) for annealed samples; opposite, X-ray data incline (7) to a value one order of magnitude lower. It should be noticed that the data reported in Ref. (6) refer mainly to samples quenched from temperatures above 550°C. Therefore, an investigation of the dependence of the inversion degree on T is desirable. We have therefore performed *in situ* powder X-ray diffraction experiments at high temperatures in the range $300 \le T \le 800$°C. The XRPD patterns at different temperatures are shown in Fig. 4. The main result is the increase in intensity of some new peaks which can be attributed to cubic $MgMn_2O_4$ (see the indexed bars at the bottom of Fig. 4. These bars refer to the cubic Mn_3O_4 since no JCPDS file of cubic $MgMn_2O_4$ is available). The coexistence of tetragonal and cubic $MgMn_2O_4$ has already been described in the literature and attributed to a kinetic effect (7). We can

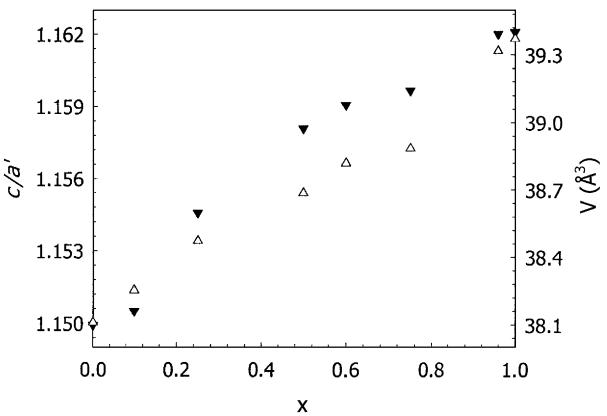

FIG. 3. Cell volume and tetragonal distortion in $Mg_{1-x}Mn_{2+x}O_4$ for $0 \le x \le 1$. Black triangles down: c/a'; white triangles up: V.

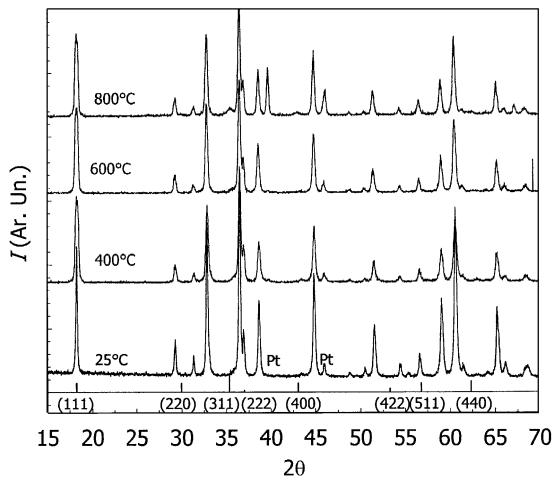

FIG. 4. XRPD patterns acquired at high-T for $MgMn_2O_4$. Reference lines correspond to the cubic Mn_3O_4.

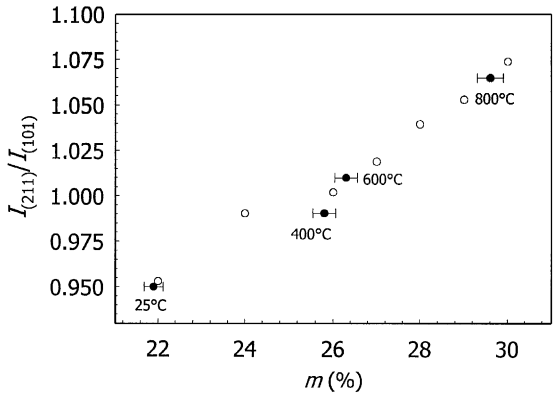

FIG. 5. Behavior of intensity ratio between (211) and (101) reflexes with T for $MgMn_2O_4$ (solid circles) and for simulated pattern with various inversion degree values (open circles).

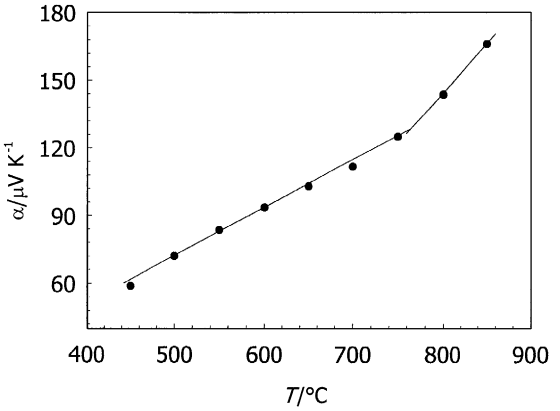

FIG. 7. Thermoelectric power (α) as a function of temperature for $MgMn_2O_4$ in air.

note here that: (a) this behavior is fully reversible, i.e. a sample fired at 1000°C and then cooled down to room temperature showed no traces of the cubic phase; and (b) the amount of the cubic phase is always quite small. From the XRPD patterns of Fig. 4 it is possible to determine the lattice constants as a function of T. It should be noted that above 600°C, the c/a' ratio for the tetragonal phase reduces progressively on increasing the temperature. This trend can be explained by the progressive replacement of Jahn–Teller Mn(III) ions on the octahedral structure sites by Mg(II) ions. Moreover it is believed that, as the inversion process takes place, charge compensation requires the formation of a Mn(IV) ion on the octahedral sites for each Mn(II) placed on the tetrahedral one (16). We may evaluate the progressive increase of the inversion process by considering the intensity of the reflections that are more sensitive to the cation exchange, that is (112), (321) and (101), and normalize them to the intensity of the (211) peak which is relatively steady with the inversion process. The normalized intensity of those three peaks show similar temperature dependencies. In Fig. 5, we presented the behavior of the integrated intensity ratios between (211) and (101) diffraction as determined by the X-ray diffraction patterns of Fig. 4 compared with the calculated intensity ratios (see the Experimental section for details). As can be seen, the inversion degree ranges from 22 to 30%; it is stable between 400 and 600°C and rises to 800°C.

The possible oxygen content deviations have been explored for $MgMn_2O_4$ by means of thermogravimetry. We measured the weight change of an $MgMn_2O_4$ sample in pure oxygen in the range $400 \leq T \leq 800$°C. The results are reported in Fig. 6. By means of reduction with hydrogen we determined that the material contains four oxygen atoms

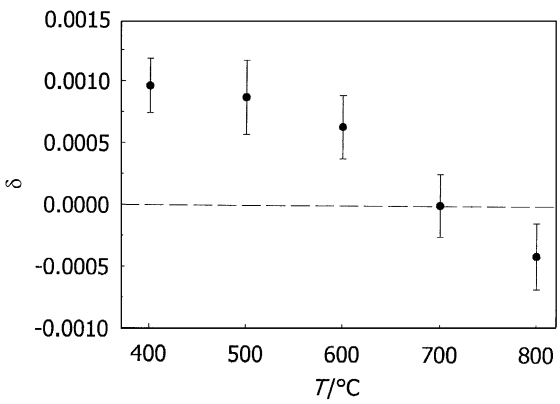

FIG. 6. Weight change in pure oxygen for $MgMn_2O_4$.

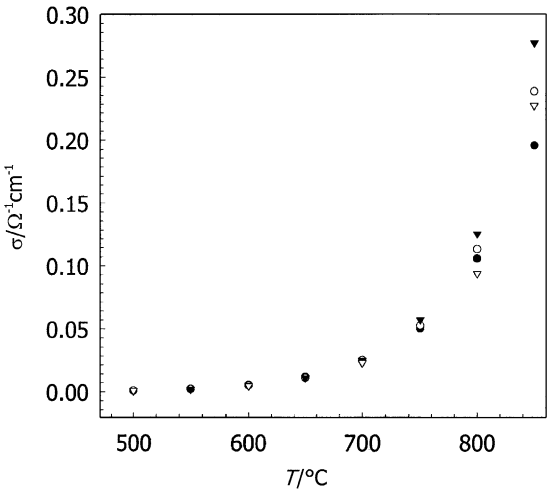

FIG. 8. Electrical conductivity (σ) vs temperature for $MgMn_2O_4$ at different oxygen partial pressures $P(O_2)$. Black squares: 1 atm; white squares: 10^{-1} atm; black triangles down: 10^{-2} atm; white triangles down: 10^{-3} atm.

per formula unit at 700°C. As can be seen, the oxygen content variation is detectable but small.

Electrical conductivity measurements have been carried out extensively on the $MgMn_2O_4$ sample. To check the different possible contributions to the electrical response the sample underwent impedance spectroscopy (IS) analysis. The spectra recorded in air at RT and in the frequency range $3.2 \times 10^{-3} \leq \omega \leq 50{,}000$ Hz show the presence of a single semicircle which allows us to conclude that the only contribution to the electrical conductivity is the bulk one. Thermoelectric power, α, measurements have been performed in air in the range $450 \leq T \leq 800$°C. The plot of α vs T is reported in Fig. 7. From the positive values of α we can conclude that $MgMn_2O_4$ is a *p*-type conductor in the whole T range considered. The presence of the kink around 700°C in the results suggests the presence of two distinct conduction regimes.

Four-probe DC electrical conductivity measurements have been performed in the range $500 \leq T \leq 850$°C and $1 \leq P(O_2) \leq 10^{-3}$ atm. The results are presented in Fig. 8. The material displays a semiconducting-like behavior at all $P(O_2)$ with conductivity increasing with increasing temperature. In addition, the data show an almost negligible dependence on oxygen partial pressure. This is a clear indication that the *main* charge carriers are not produced by defect equilibria involving oxygen defects. The activated behavior of conductivity is well revealed by the Arrhenius plots of the same data shown in Fig. 9. In all the isobaric curves a change in slope is evident at around 650°C. This is a further indication of a change in the conduction mechanism at this temperature, in agreement with the results of electric thermopower measurements. The activation energies (E_a) determined by the slope of the interpolating curves point out that the activation energies for the low-T regime (under ca. 650°C) are very slightly $P(O_2)$ dependent, with an average value of 1.1 eV. For the high-T regime the activation energy values are a little more $P(O_2)$ dependent with

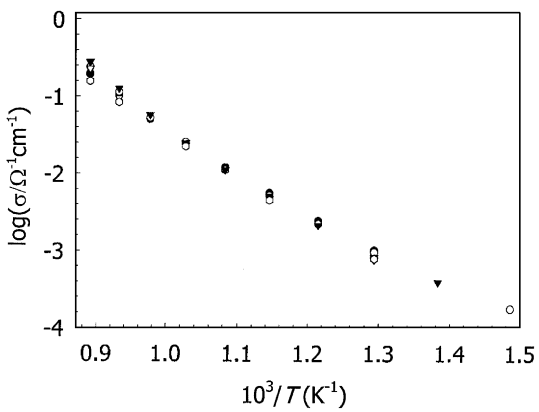

FIG. 9. Logarithm of electrical conductivity (σ) vs reciprocal temperature (Arrhenius plots) for $MgMn_2O_4$. Same data as Fig. 8.

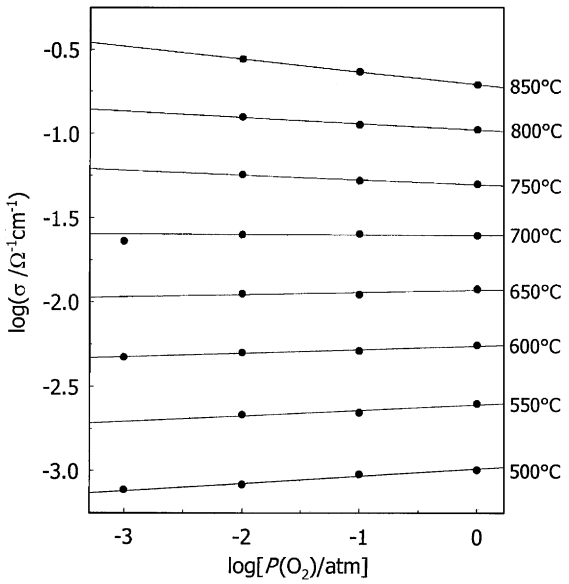

FIG. 10. Logarithm of electrical conductivity (σ) vs logarithm of the oxygen partial pressure. Same data as Fig. 9.

E_a increasing on decreasing the oxygen partial pressure from 1.3 to 1.6 eV. The log–log plot of conductivity data is presented in Fig. 10. Each set of data can be nicely interpolated by a straight line with a slope gradually changing from positive to negative being null at around 700°C. The slope of these curves is anyway very small, which to a greater extent suggests a modest dependence of transport properties from $P(O_2)$.

4. DISCUSSION

A correct understanding of $MgMn_2O_4$ transport properties requires one to think about all the possible defect equilibria which could be involved as the two thermodynamic variables, T and $P(O_2)$, are varied. We observed from diffraction, particularly from high-T data, that above 800°C a cubic phase forms (minority phase) beside the main tetragonal one. By indexing the diffraction patterns, a progressive contraction of the c/a' value for the tetragonal phase arises starting from 600°C. These findings can be understood by considering the inversion process which takes place in the $MgMn_2O_4$ spinel. This can be described, within the Kröger–Vink notation, by the following quasi-chemical equilibrium:

$$Mg_{Mg}^{x} + 2Mn_{Mn}^{x} \rightleftharpoons Mg'_{Mn} + Mn_{Mg}^{x} + Mn_{Mn}^{\cdot}. \qquad [1]$$

This process starts at around 600°C and becomes progressively more important as the temperature increases. If Eq. [1] holds, as inversion proceeds, for each Mg ion placed on an octahedral site a Mn(IV) ion forms for charge compensation. This reflects the reduction of tetragonal distortion with

temperature caused by Jahn–Teller Mn(III) ions depletion on the octahedral sites. Below 600°C, the inversion degree is constant and corresponds to one of the as-prepared samples that we estimated to be around 22%. The simultaneous presence of Mn(III) and Mn(IV) ions and the activated nature of charge carrier transport points out a hole hopping mechanism between ions of different oxidation states. This is a plausible conduction mechanism in transition metal oxides with large lattice distortions. Between 400 and 600°C, the amount of charge carrier is constant and the activation energy (1.1 eV), which is dominated by the energy required by the hopping process, is not influenced by $P(O_2)$. Above the threshold of inversion process (at about 600°C), the E_a increases since now an additional activated term is required to consider the formation process of Eq. [1]. This activation energy varies with oxygen partial pressure. The kink present in all the Arrhenius plots for the isobar curves and in the thermoelectric power graph marks the transition between the two regimes.

The effect of $P(O_2)$ on the electrical conductivity is not the dominant process in defining the transport properties of $MgMn_2O_4$ as can be seen by the small slopes found in the log–log plots (Fig. 10). In any case, the variation of slope, from positive ($T < 700$°C) to negative ($T > 700$°C), may be rationalized by coupling the thermogravimetry results and the plausible gas–solid quasi-chemical equilibria for $MgMn_2O_4$. Below 700°C, the material is slightly over-stoichiometric in the oxygen content (cf. Fig. 6) and the following equilibrium holds:

$$2O_2(\text{gas}) \rightleftharpoons 4O_O^x + V''_{Te} + 2V'''_{Oct} + 8h^{\cdot}, \qquad [2]$$

where the subscripts Oct, Te and O denote octahedral, tetrahedral and oxygen sites respectively. This extrinsic process produces charge carriers (holes) and its positive slope accounts for the progressive increase of conductivity by increasing $P(O_2)$. At around 700°C the material attains the correct oxygen content, i.e. four oxygen atoms per formula unit. Above this temperature a small oxygen under stoichiometry is present. Its effect on conductivity is opposite to the previous one since now conductivity increases on reducing $P(O_2)$. This can be written as

$$2O_O^x \rightleftharpoons O_2(\text{gas}) + 2V_O^{\cdot\cdot} + 4e'. \qquad [3]$$

It is clear that now the electrons produced, along with the oxygen vacancies, reduce the amount of charge carriers responsible for conductivity. The stronger E_a dependence on $P(O_2)$ in the high-T regime may be correlated with a $P(O_2)$ dependence of inversion. By reducing $P(O_2)$, the activation energy increases and the number of oxygen vacant sites decreases according to [3]. Even though we have no information concerning the inversion mechanism, it is likely that the cationic migration is favored by the presence of vacant sites in the anion lattice.

5. CONCLUSION

In the present paper, we present the results of the characterization of structure and transport properties of the $MgMn_2O_4$ spinel oxide. The electrical conductivity measurements can be interpreted by taking into account two defect equilibria involving (i) the inversion process and (ii) oxygen non-stoichiometry. It can be argued that the main contribution to the electrical conductivity arises from the hopping of positive charge carriers generated by inversion equilibrium. Oxygen non-stoichiometry plays a minor role because, as evidenced by thermogravimetric determination, the actual value of oxygen non-stoichiometry is very small or even negligible.

ACKNOWLEDGMENTS

This work has been partially supported by Progetto Finalizzato MSTA II. Dr. Simona Bigi is gratefully acknowledged for having performed EMPA analysis. The Department of Earth Science of Modena University and CNR of Modena are acknowledged for allowing to use the SEM. We acknowledge an anonymous referee for his valuable suggestions.

REFERENCES

1. N. Yamazoe and N. Miura, *Solid State Ion.* **86–88,** 987 (1996).
2. N. Miura, G. Lu, and N. Yamazoe, *J. Electrochem. Soc.* **143,** 2 (1996).
3. N. Miura, H. Kurosawa, H. Hasei, G. Lu, and N. Yamazoe, *Solid State Ion.* **86–88,** 1069 (1996).
4. P. Ghigna, G. Flor, and G. Spinolo, *J. Solid State Chem.* **149,** 252–255 (2000), doi: 10.1006/jssc1999.8524.
5. P. Ghigna, G. B. Barbi, G. Chiodelli, G. Spinolo, L. Malavasi, and G. Flor, *J. Solid State Chem.* **153,** 231–236 (2000), doi: 10.1006/jssc2000.8746.
6. N. K. Radhakrishnan and A. B. Biswas, *Phys. Stat. Sol.* **37,** 719–722 (1976).
7. R. Manaila and P. Pausescu, *Phys. Stat. Sol.* **9,** 385–392 (1965).
8. G. Spinolo and F. Maglia, *Powder Diffraction* **14,** 208–212 (1999).
9. G. Chiodelli and P. Lupotto, *J. Electrochem. Soc.* **138,** 2703–2711 (1991).
10. M. Scavini, G. Chiodelli, G. Spinolo, and G. Flor, *Physica C* **230,** 412–418 (1994).
11. J. Rodriguez-Carvajal, *Physica B* **192,** 55–69 (1993).
12. W. Kraus and G. Nolze, *J. Appl. Crystallogr.* **29,** 301–303 (1996).
13. A. P. Shina, N. R. Sanjana, and A. B. Biswas, *Acta Crystallogr.* **10,** 439–445 (1957).
14. C. B. Azzoni, M. C. Mozzati, L. Malavasi, P. Ghigna, and G. Flor, *Solid State Commun.* **119,** 591–595 (2001).
15. C. B. Azzoni, M. C. Mozzati, P. Ghigna, L. Malavasi, and G. Flor, *Solid State Commun.* **117,** 511–515 (2001).
16. M. Rosemberg and P. Nicolau, *Phys. Stat. Sol.* **6,** 101–110 (1964).